JCTC Journal of Chemical Theory and Computation

Article

pubs.acs.org/JCTC

Thermodynamical Description of a Quasi-First-Order Phase Transition from the Well-Tempered Ensemble

Omar Valsson* and Michele Parrinello

Department of Chemistry and Applied Biosciences, ETH Zurich, and Facoltà di Informatica, Instituto di Scienza Computationali, Università della Svizzera italiana, Via Giuseppe Buffi 13, CH-6900 Lugano, Switzerland

Supporting Information

ABSTRACT: We explore the performance of the well-tempered ensemble combined with parallel tempering (PT-WTE) in obtaining a thermodynamical description of a given molecular system. We carefully explain the theoretical procedure employed to extract all the relevant thermodynamical quantities from a PT-WTE simulation. As a specific molecular system, we consider a Lennard−Jones cluster of 147 particles, which is a prototypical case of a finite-size system exhibiting a quasi-first-order phase transition, characterized by a range of temperatures where two distinct phases are thermodynamically stable and coexist. Two separate PT-WTE simulations, which investigate the thermodynamical behavior on different levels of detail, give equally accurate descriptions of the critical phase-coexistence region, indicating the good quality of the PT-WTE results. The positive performance observed here clearly demonstrates that the PT-WTE approach is an effective option when thermodynamical properties are needed.

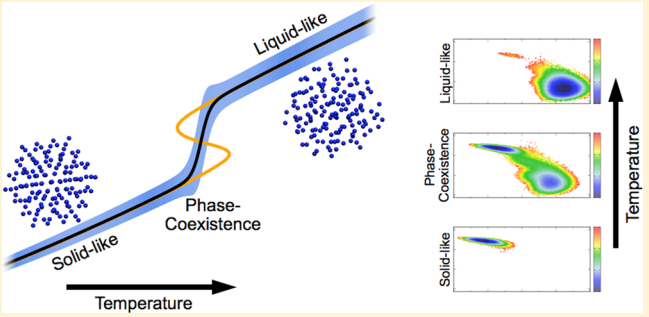

1. INTRODUCTION

From the density of states of any given molecular system, the full spectrum of thermodynamical properties can be obtained. However, obtaining a reliable estimate of the density of states from molecular simulations is a highly demanding task as it requires an extensive sampling of configurational space.

One method that has proven efficient in this respect is the Wang−Landau Monte Carlo approach.[1] This approach builds an estimate of the density of states, which is employed to bias the Monte Carlo sampling such that previously explored configurations are less likely to be revisited. In the long time limit, the Wang−Landau approach effectively samples the multicanonical ensemble,[2] which is a generalized ensemble where the effective potential energy probability distribution is complete flat, such that all potential energies are equally probable. Another closely related approach is statistical temperature molecular dynamics,[3] which can be considered to extend the ideas of the Wang−Landau method to molecular dynamics (MD).

The well-tempered ensemble[4] (WTE), recently introduced in our group, has some similarities to the Wang−Landau approach. Specifically, the WTE is obtained when the potential energy is employed as a collective variable in the well-tempered[5] variant of metadynamics.[6] In the WTE, we build a biasing potential that hinders visiting previously explored configurations, which in the long time limit provides an estimate of the free energy as function of the potential energy. Different from the Wang−Landau approach, the WTE converges to an effective probability distribution that is not completely flat but rather is amplified as compared to the canonical one. The amplification depends on an adjustable parameter, allowing the deviation from the canonical ensemble to be controlled.

So far, the performance of the WTE in estimating the density of states has not been explored. In view of previous studies,[7,8] which employed regular metadynamics in combination with the potential energy, we already expect the WTE to be efficient for this purpose, especially because the well-tempered variant of metadynamics has a well-defined convergence limit that the regular variant lacks.

Here, we will explore the performance of the WTE in estimating the density of states and thereby obtaining a complete thermodynamical description of a given system. We solely focus our attention on the combination of the WTE with parallel tempering[9,10] (PT-WTE), as it has shown to be a rather efficient combination.[4,11] As a benchmark case, we consider a Lennard−Jones cluster of 147 particles (LJ147). This cluster, and other Lennard−Jones clusters, have been extensively studied as they are prototypical examples of finite-size systems exhibiting the analog of a first-order phase transition (see ref 12 and references there-in). We designate such phase transitions as quasi-first-order phase transitions in order to distinguish them from their true (bulk) counterparts that are only defined in the thermodynamic limit. The behavior of such finite-size systems is quite different from the bulk; instead of having a single

Received: October 1, 2013
Published: November 15, 2013

transition or melting temperature, there is a range of temperatures where two distinct phases are thermodynamically stable and coexist dynamically.[13] For example, such behavior has been experimentally observed in small sodium clusters.[14] A closely related issue is the fact that in molecular simulations of periodic systems with small unit cells, the system can easily go between an ordered and a disordered state, an effect that has efficiently been employed to search for candidate structures of molecular solids.[15,16]

The structure of the paper is as follows. In Section 2, we review the properties of the WTE and carefully explain the procedure employed to extract the thermodynamical quantities from a PT-WTE simulation. We then briefly review the characteristics of a quasi-first-order phase transition in Section 3. The computational details of the simulations are given in Section 4. In Section 5, we present our results for the Lennard–Jones cluster and finally conclude in Section 6.

2. BACKGROUND AND THEORY

2.1. The Well-Tempered Ensemble. We consider a system of N particles at constant volume V, which is characterized by some potential energy function $U(\mathbf{R})$. In the canonical ensemble at temperature T (with $\beta = (k_B T)^{-1}$ as usual), the probability distribution for the potential energy U is obtained by weighting the configurational density of states $N_c(U) = \int d\mathbf{R}\delta(U-U(\mathbf{R}))$ with the Boltzmann factor $e^{-\beta U}$

$$P_c(U;T) = \frac{e^{-\beta U}N_c(U)}{Z_c(T)} \tag{1}$$

where $Z_c(T) = \int dU e^{-\beta U}N_c(U)$ is the configurational partition function.

Employing the potential energy $U = U(\mathbf{R})$ as a collective variable in well-tempered metadynamics[5] results in an generalized ensemble appropriately named the well-tempered ensemble.[4] In the WTE, there is an additional time-dependent biasing potential $V(U,t)$ that depends on U and discourages the system from visting previously explored configurations. The time evolution of the biasing potential is given by

$$\dot{V}(U,t) = \omega e^{-V(U,t)/k_B\Delta T}\delta_{U,U(t)} \tag{2}$$

where ω is the initial energy deposition rate, and ΔT is a parameter with the dimensionality of a temperature. In practice, the biasing potential is expressed as a sum of Gaussians of width $\sigma_{G,U}$ that are deposited with time interval τ_G

$$V(U,t) = \sum_{t'=0,\tau_G,2\tau_G,\ldots}^{t'\le t} W_G e^{-V(U(t'),t')/k_B\Delta T} e^{\left(-\frac{(U-U(t'))^2}{2\sigma_{G,U}^2}\right)} \tag{3}$$

where the initial height is given by $W_G = \omega\tau_G$.

It is clear that the time evolution term in eq 2 will tend to zero as the simulation proceeds, so the time-dependent biasing potential will quickly become constant in time and converge to its long time limit. It can be shown that this limit gives an unbiased estimate of the free energy as function of the potential energy[5]

$$V(U,t\to\infty;T) = -(1-\gamma^{-1})F_c(U;T) \tag{4}$$

where the biasing factor is defined as $\gamma = (T+\Delta T)/T$. We will call this the configurational free energy in order to distinguish it from the free energy as function of the total energy $F(E;T)$, which we discuss later on. The configurational free energy is formally defined as

$$F_c(U;T) = -\beta^{-1}\ln\frac{\int d\mathbf{R}\delta(U-U(\mathbf{R}))e^{-\beta U(\mathbf{R})}}{\int d\mathbf{R}e^{-\beta U(\mathbf{R})}} \tag{5}$$

which up to an unimportant constant can be written as

$$F_c(U;T) = U - \beta^{-1}\ln N_c(U) \tag{6}$$

In the long time limit, the dynamics of the system is determined by an effective potential $U_\gamma(\mathbf{R})$, which is the sum of the normal potential energy function $U(\mathbf{R})$ and the biasing potential $V(U,t\to\infty;T)$

$$\begin{aligned} U_\gamma(\mathbf{R}) &= U(\mathbf{R}) - (1-\gamma^{-1})[U(\mathbf{R}) - \beta^{-1}\ln N_c(U(\mathbf{R}))] \\ &= \gamma^{-1}U(\mathbf{R}) + \beta^{-1}(1-\gamma^{-1})\ln N_c(U(\mathbf{R})) \end{aligned} \tag{7}$$

Therefore, $N_c(U)$ will now be weighted by a modified Boltzmann factor $e^{-\beta U_\gamma}$, so the effective potential energy probability distribution in the WTE is

$$\begin{aligned} P_{c,\gamma}(U;T) &= \frac{e^{-\beta U_\gamma}N_c(U)}{Z_{c,\gamma}(T)} \\ &= \frac{[e^{-\beta U}N_c(U)]^{1/\gamma}}{Z_{c,\gamma}(T)} \\ &= \frac{[Z_c(T)P_c(U;T)]^{1/\gamma}}{Z_{c,\gamma}(T)} \\ &\propto [P_c(U;T)]^{1/\gamma} \end{aligned} \tag{8}$$

where $Z_{c,\gamma}(T) = \int dU[e^{-\beta U}N_c(U)]^{1/\gamma}$ is the configurational partition function in the WTE, and $P_c(U;T)$ is the potential energy probability distribution in the canonical ensemble. This clearly shows the main property of the WTE; it is a generalized ensemble that compared to the canonical ensemble has a modified potential energy probability distribution given by $P_{c,\gamma}(U;T)\propto[P_c(U;T)]^{1/\gamma}$, while the kinetic energy probability distribution is the same as in the canonical ensemble. Therefore, by adjusting value of γ employed in the WTE, we can selectively enhance the sampling of configurations.

It is instructive to compare the WTE to another well-known generalized ensemble, the multicanonical ensemble.[2] In the multicanonical ensemble, the effective potential energy probability distribution $P_{mc}(U;T) = constant$ is completely uniform as function of the potential energy U and temperature T. However, in the WTE, the effective potential energy probability distribution $P_{c,\gamma}(U;T) \propto [P_c(U;T)]^{1/\gamma}$ still varies with the potential energy U and temperature T but becomes more uniform as γ increases. Then, in the limit $\gamma\to\infty$, which corresponds to regular (non-well-tempered) metadynamics,[6] the probability distribution becomes completely constant, $P_{c,\gamma}(U;T) = constant$, and the WTE becomes equivalent to the multicanonical ensemble. Of course, it is obvious that the limit $\gamma\to 1$ corresponds to the canonical ensemble.

To say more on the behavior in the WTE requires us to assume some form of potential energy probability distribution in the canonical ensemble. In many cases, like for explicitly solvated systems, $P_c(U;T)$ is unimodal and close to its maximum can be numerically approximated by a Gaussian

distribution.[17] In this case, the potential energy probability distribution in the canonical ensemble is given by

$$P_c(U;T) \propto e^{-\langle U\rangle^2/2\sigma_U^2} \tag{9}$$

where $\langle U\rangle$ and σ_U^2 are the average and variance, respectively, of the potential energy at some temperature T. In the WTE, the potential energy probability distribution is then given by

$$P_{c,\gamma}(U;T) \propto [P_c(U;T)]^{1/\gamma} \propto e^{-\langle U\rangle^2/2\gamma\sigma_U^2} \tag{10}$$

that is, a Gaussian distribution with the average $\langle U\rangle$ and variance $\gamma\sigma_U^2$. Therefore, for not too large values of γ, we can expect to obtain the same average potential energy as in the canonical ensemble but with an enhanced variance that should increase linearly with γ. For larger values of γ, we can expect deviations from this behavior as then we start to go further into the tails of $P_c(U;T)$, where the Gaussian approximation is no longer valid.

For a quasi-first-order phase transition in a finite-size system, like the one we consider in the current work, the behavior is quite different. As discussed in more detail in Section 3, the canonical potential energy probability distribution can be bimodal in a finite temperature range, corresponding to the fact that two distinct phases are thermodynamically stable. In Figure 1, we illustrate the behavior of the WTE for this case by considering a hypothetical system where $P_c(U;T)$ is given as sum of two Gaussians, which is a fairly reasonable assumption for a quasi-first-order phase transition (see Figure 2 in Section 5). We observe that the WTE results in an enhancement in the fluctuations of each phase and a broadening of the peaks. Furthermore, there will be a reduction in the free energy barrier between the two phases, so transitions between the phases should become more frequent.

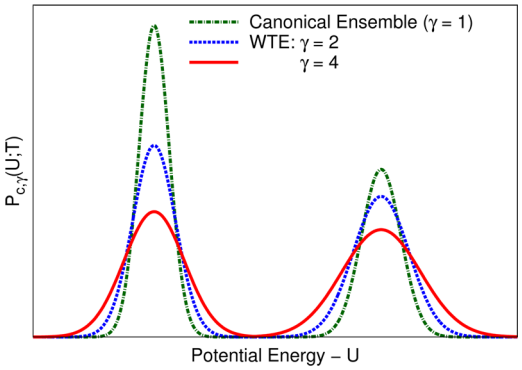

Figure 1. Potential energy probability distributions $P_{c,\gamma}(U;T)$ in the WTE for a hypothetical system where the canonical potential energy probability $P_c(U;T)$ is given as sum of two Gaussian, which is a fairly reasonable assumption for a quasi-first-order phase transition (see Figure 2 in Section 5).

2.2. Parallel Tempering and WTE. Any generalized ensemble can be combined with the parallel tempering (PT) approach,[9,18] and for the WTE this has been shown to yield a rather efficient combination.[4,11] In conventional PT, we have M replicas at different temperatures $T_1 < T_2 < ... < T_M$ and for each replica perform a simulation in canonical ensemble. On the basis of the Metropolis acceptance criterion, the PT approach will at fixed intervals try an exchange of configurations between two neighboring replicas. In order to preserve detailed balance, the acceptance probability for the exchange of configurations $\mathbf{R}_i$ and $\mathbf{R}_r$ between two neighboring replicas with temperatures T_i and T_r, respectively, is given by

$$p(i \to r) = \min(1, e^{\Delta_{i,r}}) \tag{11}$$

where

$$\Delta_{i,r} = (\beta_i - \beta_r)(U_i - U_r) \tag{12}$$

with $U_i = U(\mathbf{R}_i)$ and $U_r = U(\mathbf{R}_r)$ as the potential energies of replicas i and r, respectively. It is clear from the above equation, that in order to have appreciable probability for the exchange, the potential energy probability distributions of the two replicas, $P_c^{(i)}(U;T_i)$ and $P_c^{(r)}(U;T_r)$, will need to overlap sufficiently. For a constant temperature range, the number of replicas needed to fullfil this requirement goes as the square root of system size (i.e., the number of degrees of freedom),[19] making conventional PT very expensive for large systems.

In PT combined with the WTE, the simulation of each replica is instead performed in the WTE. Each replica i is then characterized by a biasing potential $V_G^{(i)}(U,t)$, which has a long time limit

$$V_G^{(i)}(U,t \to \infty;T_i) = -(1 - \gamma_i^{-1})(U - \beta_i^{-1}\ln N_c(U)) \tag{13}$$

and a potential energy probability distribution given by

$$P_{c,\gamma}^{(i)}(U;T_i) \propto [P_c^{(i)}(U;T_i)]^{1/\gamma_i} \tag{14}$$

Therefore, as compared to conventional PT, there is an enhanced overlap of the probability distributions so the likelihood of an exchange between replicas will be increased.

Furthermore, at every exchange attempt, the acceptance probability in PT-WTE is determined by[20]

$$\begin{aligned}\Delta_{i,r} = {} & (\beta_i - \beta_r)(U_i - U_r) + \beta_i[V_G^{(i)}(U_i,t) - V_G^{(i)}(U_r,t)] \\ & + \beta_r[V_G^{(r)}(U_r,t) - V_G^{(r)}(U_i,t)]\end{aligned} \tag{15}$$

where the additional terms come from the fact that the two replicas have different biasing potentials. The biasing potentials will converge to their long time limits, so effectively $\Delta_{i,r}$ can be written as

$$\begin{aligned}\Delta_{i,r} = {} & (\beta_i - \beta_r)(U_i - U_r) \\ & - \beta_i(1 - \gamma_i^{-1})[U_i - \beta_i^{-1}\ln N_c(U_i) - U_r \\ & \quad + \beta_i^{-1}\ln N_c(U_r)] \\ & - \beta_r(1 - \gamma_r^{-1})[U_r - \beta_r^{-1}\ln N_c(U_r) - U_i \\ & \quad + \beta_r^{-1}\ln N_c(U_i)] \\ = {} & (\beta_i\gamma_i^{-1} - \beta_r\gamma_r^{-1})(U_i - U_r) - (\gamma_i^{-1} - \gamma_r^{-1})\ln\frac{N_c(U_i)}{N_c(U_r)}\end{aligned} \tag{16}$$

In most cases, we would employ the same biasing factor for all replicas, $\gamma_i = \gamma_r = \gamma$, so the second term vanishes and we obtain

$$\Delta_{i,r} = \gamma^{-1}(\beta_i - \beta_r)(U_i - U_r) \tag{17}$$

Thus, as compared to conventional PT, $\Delta_{i,r}$ is reduced by a factor of γ, which enhances the exchange probability.

Therefore, the PT-WTE approach has two properties that make it more favorable than PT in the canonical ensemble: the enhanced overlap of potential energy probability distributions between replicas and the reduction in $\Delta_{i,r}$, both of which

depend directly on the biasing factor γ. Thus, by adjusting the biasing factor γ, we can adapt the PT-WTE approach to the problem at hand.

2.3. Thermodynamical Quantities from WTE. For thermodynamical properties, the relevant quantity is the density of states as a function of the total energy, $N(E)$. In the following, we show how this quantity can be estimated from the configurational free energy $F_c(U;T)$. We will then show how the total density of states $N(E)$ (or more exactly, the total entropy $S(E)$) can be employed to obtain the all the relevant thermodynamical quantities.

Up to an unimportant constant, the configurational free energy $F_c(U;T)$ at temperature T is given by

$$F_c(U;T) = U - \beta^{-1}\ln N_c(U) = U - TS_c(U) \tag{18}$$

where $S(U) = k_B \ln N_c(U)$ is the configurational entropy of the system. Similarly, the total free energy as a function of E is given by

$$F(E;T) = E - \beta^{-1}\ln N(E) = E - TS(E) \tag{19}$$

where $S(E) = k_B \ln N(E)$ is the total entropy of the system. It is clear that the entropy provides the same information as the density of states, so the two quantities can be used interchangeably. It is normally more convenient to work with the entropy, so in the following, we consider only the entropy and not the density of states directly.

The total free energy $F(E;T)$ can be obtained from the configurational free energy $F_c(U;T)$ by employing the fact that the probability distribution for the total energy $E = U + K$ is given by a convolution of the potential and kinetic energy probability distributions[12]

$$P(E;T) = \int_0^E \mathrm{d}K P_c(E - K;T)P_m(K;\, T) \tag{20}$$

where we take the zero of the energy to be the global minimum on the potential energy surface. The probability distribution for the potential energy can be estimated from the configurational free energy $F_c(U;T)$ as

$$P_c(U;T) = \frac{e^{-\beta F_c(U;T)}}{\int \mathrm{d}U' e^{-\beta F_c(U';T)}} \tag{21}$$

while the probability distribution for the kinetic energy K is analytically known and is given by a Gamma distribution[12]

$$P_m(K;T) = \frac{\beta^{\kappa/2}K^{\kappa/2-1}e^{-\beta K}}{\Gamma(\kappa/2)} \tag{22}$$

where κ is the number of degrees of freedom (normally $\kappa = 3N - 6$ or $\kappa = 3N - 3$, depending on if the angular momentum is kept fixed or not, respectively). Subsequently, the total free energy $F(E;T)$ can be obtained as

$$F(E;T) = -k_B T \ln P(E;T) \tag{23}$$

We can obtain an estimate of the total entropy from the total free energy $F(E;T)$ as

$$S(E) = \frac{F(E;T) - E}{T} \tag{24}$$

However, this estimate will only be valid for the region of E where the corresponding configurational free energy $F_c(U;T)$ has been sufficiently sampled, which depends mainly on T but also the biasing factor γ. Therefore, we need to combine estimates of $S(E)$ from different PT-WTE replicas in order to obtain an estimate valid for a wider region of E than obtained from a single PT-WTE replica. In the following section, we will describe our procedure for accomplishing this, but for now, we assume that we know $S(E)$ for the complete region of interest.

Once the total entropy $S(E)$ is known, the canonical temperature average of any function $f(E)$ that depends on the total energy E is obtained as

$$\langle f(E)\rangle(T) = \frac{\int \mathrm{d}E' f(E') e^{S(E)/k_B - E'/k_B T - b}}{\int \mathrm{d}E' E e^{S(E)/k_B - E'/k_B T - b}} \tag{25}$$

where, to avoid numerical problems, we subtract a constant $b = \max[S(E)/k_B - E'/k_B T]$, both from the numerator and denominator. We can employ this equation to obtain the canonical caloric curve $\langle E\rangle(T)$, which gives the average total energy in the canonical curve as a function of temperature. Furthermore, the variance of the total energy is obtain from this equation as $\sigma_E^2(T) = (\langle E^2\rangle(T) - \langle E\rangle^2(T))$, from which we can then obtain the canonical specific heat at constant volume as

$$C_V(T) = \frac{\partial\langle E\rangle(T)}{\partial T} = \frac{\sigma_E^2(T)}{k_B T^2} \tag{26}$$

The microcanonical caloric curve $T(E)$, which gives the average temperature in the microcanonical ensemble as a function of the fixed total energy E, can be obtained from the total entropy $S(E)$ as

$$T(E) = \left[\frac{\partial S(E)}{\partial E}\right]^{-1} \tag{27}$$

In the same manner, the configurational entropy $S_c(U)$ can be employed to obtain the isopotential caloric curve as $T_c(U) = [\partial S_c(U)/\partial U]^{-1}$, which gives the average temperature in the so-called isopotential ensemble, where only the potential energy is kept fixed while the kinetic energy allowed to vary.[12]

Because of the finite width of the Gaussian employed to build the biasing potential and the statistical fluctuations, there will always be some noise in the configurational free energies $F_c(U;T)$ obtained from a PT-WTE simulation. Now, the kinetic energy probability distribution $P_m(K;T)$ is an unimodal function, which in most cases is almost indistinguishable from a normal distribution (unless the number of degrees of freedom κ is very small). Therefore, the convolution in eq 20 should result in a considerable reduction of the noise in $F_c(U;T)$, such that the total free energies $F(E;T)$ will be much smoother and free of noise (as clearly is shown by comparing Figure 2 below with Figure S2 in the Supporting Information). The benefit of this noise reduction is clearly noticeable in a microcanonical caloric curve $T(E)$ in Figure 2, which is very smooth and completely noise-free, while the corresponding isopotential caloric curve $T_c(U)$ in Figure S2 in the Supporting Information is much more noisy.

A further effect of the convolution is that the total energy probability distributions $P(E;T)$ will in general have broader peaks than the corresponding potential energy probability distributions $P_c(U;T)$, so the free energy barriers in the total free energies $F(E;T)$ will be smaller than the barriers in the corresponding configurational free energies $F_c(U;T)$.

2.4. Combining Results from Different PT-WTE Replicas. As discussed in the previous section, we obtain from each replica in a PT-WTE simulation, an estimate of the total entropy $S(E)$ valid for the region of the total energy E

explored in that replica. As required in PT, there will be an overlap of E for neighboring replicas, so we can combine the different estimates and obtain an estimate of the total entropy $S(E)$ valid for the complete region of E explored in the PT-WTE simulation. However, $S(E)$ is only determined up to a constant, so the different estimates will differ by some unknown constants and therefore cannot be directly combined. In the weighted histogram analysis method (WHAM),[21] this is solved by determining the unknown constants in an iterative fashion. Recently, a different approach to this problem has been presented, the so-called statistical temperature weighted histogram analysis method (ST-WHAM),[22,23] which has the advantage of being an iteration free method. This methods employs the fact that the microcanonical caloric curve $T(E)$ (i.e., the derivative of $S(E)$) will be free of any unknown constant, and therefore, the different estimates of $T(E)$ can be combined directly. The total entropy $S(E)$ can then be obtained by integrating the combined $T(E)$ curve.

In the present work, we employ a procedure that is similar in spirit to the ST-WHAM method and is described in the following. We consider a PT-WTE simulation with M replicas at different temperatures T_i ($i = 1,...,M$), which explore overlapping regions of E and yield estimates of the configurational free energies $F_c(U;T_i)$. For each replica i, we obtain from $F_c(U;T_i)$ estimates of the total energy probability distribution $P(E;T_i)$, total free energy $F(E;T_i)$, total entropy $S_i(E)$, and microcanonical caloric curve $T_i(E)$ (see the previous section for how to obtain these estimates). Now, the microcanonical caloric curve $T(E)$ has no unknown constant, so we can combine the different estimates $T_i(E)$ directly and obtain the complete microcanonical caloric curve as a weighted sum

$$T(E) = \sum_{i=1,...,M} w_i(E) T_i(E) \tag{28}$$

where the weights $w_i(E)$ are proportional to $P(E;T_i)$ and normalized to one

$$w_i(E) = \frac{P(E;T_i)}{\sum_j P(E;T_j)} \tag{29}$$

The total entropy $S(E)$ is then obtained by integrating the inverse of $T(E)$

$$S(E) = \int_{E_{min}}^{E} dE' \frac{1}{T(E')} \tag{30}$$

where E_{min} is chosen as the lower limit of the total energies explored in the PT-WTE simulation.

If needed, this procedure can also be employed to combine different estimates of the isopotential caloric curve $T_c(U)$ and obtain an estimate of the configurational entropy $S_c(U)$ (in this case, $P(E;T_i)$ would be replaced by $P_c(U;T_i)$). Furthermore, this procedure can also be applied to independent WTE simulations, given that there is sufficient total energy overlap between different simulations.

2.5. Summary of the Simulation Procedure. In summary, our procedure for obtaining the thermodynamical quantities from a PT-WTE simulation consists of the following steps:

(1) Perform a PT-WTE simulation employing M replicas at temperatures $T_1 < T_2 < ... < T_M$ and a biasing factor γ. The simulation is stopped once the WTE biasing potential for each replica has converged to its long time limit $V(U,t \to \infty;T_i) = -(1-\gamma^{-1})F_c(U;T_i)$. This will always be the most time-consuming part of the procedure.

(2) Obtain the configurational free energies $F_c(U;T_i)$ from the WTE biasing potentials. For each replica, we then obtain an estimate of the potential energy probability distribution $P_c(U;T_i)$.

(3) For each replica, obtain the total energy probability distribution $P_i(E;T_i)$ by performing a convolution of the potential and kinetic energy probability distributions $P_c(U;T_i)$ and $P_m(K;T_i)$. We then obtain the total free energy $F(E;T_i)$ from $P(E;T_i)$, and subsequently estimates of the total entropy $S_i(E)$ and microcanonical caloric curve $T_i(E)$.

(4) Obtain the complete microcanonical caloric curve $T(E)$ by combining the estimates $T_i(E)$ from the different replicas. The complete estimate of the total entropy $S(E)$ is then obtained by integrating $T(E)$. From $S(E)$, we compute the canonical caloric curve $\langle E \rangle(T)$, variance of the total energy $\sigma_E^2(T)$, and specific heat $C_v(T)$.

3. QUASI-FIRST-ORDER PHASE TRANSITIONS IN FINITE-SIZE SYSTEMS

Finite-size systems, like small atomic and molecular clusters, can exhibit a melting behavior rather different from their bulk counterparts.[12] First, for such systems, the definition of a solid and a liquid state might not always be straightforward, and perhaps it is more proper to talk about the solid-like and liquid-like states or even ordered and disordered states. Second, first-order and second-order phase transitions are only well defined in the thermodynamic limit $N \to \infty$, so employing such classifications for finite-size system can be ambiguous.

Nevertheless, some phase transitions in a small finite-size system can best be described as quasi-first-order phase transitions as they show some similarities to a proper first-order phase transition in the bulk. For such phase transitions, there is not a well-defined melting or transition temperature but rather a range of temperatures where both phases are thermodynamically stable and can coexist.[13] Here, we can define the lowest temperature where the liquid-like phase is thermodynamically stable as the freezing temperature T_f and the highest temperature where solid-like phase is thermodynamically stable as the melting temperature T_m. For the phase coexistence, we have to consider an ensemble of clusters that are divided into either completely solid-like or liquid-like states, with the relative ratio of the two phases determined by the canonical probability distribution at that temperature. For a single cluster, this will be observed as a dynamical phase coexistence, where over time, the cluster undergoes transitions between entirely solid-like and liquid-like states.

Quasi-first-order phase transitions are recognizable by the behavior of the thermodynamical quantities in the phase coexistence region.[12] In the temperature range from T_f to T_m, both the solid-like and liquid-like phases are thermodynamically stable, so the total free energy $F(E;T)$ will have two minima and the total energy probability distribution $P(E;T)$ will be bimodal. Furthermore, due to the enhanced fluctuations of the total energy, the specific heat $C_v(T)$ should be peaked in the temperature range from T_f to T_m. Another sign is that the microcanonical caloric curve $T(E)$ will not be a monotonically increasing function but instead will be characterized by a so-called S-bend with turning points at the freezing and melting temperatures (T_f and T_m). This means that in the microcanonical ensemble there will be three values of total energy E with the same average temperature T for $T_f < T < T_m$.

dx.doi.org/10.1021/ct400859f | J. Chem. Theory Comput. 2013, 9, 5267−5276

It is important to note that the presence of a S-bend in the isopotential caloric curve $T_c(U)$ is a required but not sufficient condition for a S-bend in the microcanonical caloric curve $T(E)$ and that the S-bends in the two curves will not have the same turning points.[12,24] Furthermore, it is clear that for the total energy probability distribution $P(E;T)$ to be bimodal the corresponding potential energy probability distribution $P_c(U;T)$ must also be bimodal (see eq 20 above).

4. COMPUTATIONAL DETAILS

We consider a finite-size cluster of 147 identical particles that interact via a Lennard–Jones (LJ) pair potential.[25] As usual when considering Lennard–Jones systems, we work in reduced units such that the Lennard–Jones parameters σ and ε, atomic mass m, and Boltzmann factor k_B are taken to be equal to one. Therefore, all lengths and energies are given in units of σ and ε, respectively, while time is given in units of $t^* = (\varepsilon/m\sigma^2)^{1/2}$ and temperature in units of $T^* = k_BT/\varepsilon$. All energy values are given relative to the global minimum of the LJ147 cluster from ref 26.

All molecular dynamics (MD) simulations are performed with the Gromacs 4.5.5[27] code, patched with the PLUMED 2.0[28] metadynamics code. We employ a time step of 0.001 t^* and keep a constant temperature using the velocity rescaling thermostat[29] (relaxation time of 0.1 t^*). We use no cutoffs for the LJ interactions and perform the simulations in vacuum. In order to prevent evaporations of the cluster, we employ a confinement potential of the form $V_c(r) = k(r-r_0)^4$ that only acts on a particle if r, the distance of the particle from the cluster center of mass, is larger than r_0. We employ the values $k = 100\ \varepsilon$ and $r_0 = 3.5\ \sigma$ for all simulations.

The parameters for the PT-WTE simulations are as follows. We deposit a Gaussian every 1000 steps or $t_G = 1.0\ t^*$ and try an exchange of replicas every 10000 steps or 10.0 t^*. The height of the Gaussian is selected to be $W_G = 0.03\ \varepsilon$, which is roughly 1/10th of k_BT for the T inside the phase coexistence region (which is around temperatures of 0.35–0.38 T^*). The width of the Gaussian is chosen to be $\sigma_{G,U} = 2.0\ \varepsilon$, which is approximately one-fourth of the standard deviation of the potential energy for the solid-like phase at a temperature of 0.30 T^*. We perform two different PT-WTE simulations, identified as **LJ147-1** and **LJ147-2**. In the **LJ147-1** simulation, we consider five replicas in the temperature range from 0.34 T^* to 0.38 T^* and employ a biasing factor of $\gamma = 2$. The temperatures of the replicas are selected to be equispaced (0.34 T^*, 0.35 T^*, 0.36 T^*, 0.37 T^*, 0.38 T^*). For the **LJ147-2** simulation, we consider 11 replicas in the temperature range from 0.20 T^* to 0.45 T^* and employ a biasing factor of $\gamma = 5$. The temperatures of the replicas are selected from a geometric distribution (0.200 T^*, 0.217 T^*, 0.235 T^*, 0.255 T^*, 0.277 T^*, 0.300 T^*, 0.325 T^*, 0.353 T^*, 0.383 T^*, 0.415 T^*, 0.450 T^*). The **LJ147-1** and **LJ147-2** simulations are both run for a time of $6 \times 10^5\ t^*$. Unless otherwise specified, all curves presented in the Results section are obtained by employing data taken at a time of $5 \times 10^5\ t^*$ (see the Supporting Information for discussion on the error bars for these curves), while numerical estimates along with their error bars are obtained by averaging over the last $1 \times 10^5\ t^*$ part of the simulations (from a time of $5 \times 10^5\ t^*$ to $6 \times 10^5\ t^*$, see Figure S7, Supporting Information).

5. RESULTS

As the benchmark system for our PT-WTE simulations, we consider a Lennard–Jones cluster of 147 particles (LJ147) that has previously been investigated as a prototypical case of a quasi-first-order phase transition.[24,30] The most difficult part is obtaining an accurate description of the phase coexistence region, as free energy barriers might hinder proper sampling of the two thermodynamically stable phases in molecular simulations of finite time. Therefore, in the following, we will consider two PT-WTE simulations that investigate the phase coexistence region on different levels of detail. In the simulation labeled **LJ147-1**, we employ densely spaced replicas in a narrow temperature range that covers the phase coexistence region. This allows us to carefully characterize the phase coexistence region and, furthermore, obtain accurate reference results for our second simulation. In the PT-WTE simulation labeled **LJ147-2**, we consider a much larger temperature range to obtain the complete thermodynamical behavior of the LJ147 cluster. Still, despite the more sparsely placed replicas, this simulation provides as good a description of the phase coexistence region as the more focused **LJ147-1** simulation.

5.1. Phase Coexistence Region. In unbiased MD simulations at temperatures around 0.35 T^* to 0.37 T^*, the LJ147 cluster exhibits a dynamical phase coexistence where it undergoes infrequent transitions between solid-like and liquid-like states (see Figure S1, Supporting Information, for results obtained at a temperature of 0.36 T^*). Therefore, in order to carefully characterize the phase coexistence region, we will initially focus on this temperature range and consider the results from the **LJ147-1** simulation. In this simulation, we employ five replicas that have equispaced temperatures in the range from 0.34 T^* to 0.38 T^* and a biasing factor of $\gamma = 2$.

In Figure 2, we present the total free energies ($F(E;T)$) and the total energy probability distributions ($P(E;T)$) obtained from the **LJ147-1** simulation (the corresponding configurational quantities are shown in Figure S2, Supporting Information). For the replica at a temperature of 0.36 T^*, the two free energy minima, corresponding to the solid-like and liquid-like phases, have almost equal free energies (there is less than 0.05 ε difference between the two minima) but are separated by a free energy barrier of around $0.7\ \varepsilon \approx 2.0\ k_BT$. Therefore, at this temperature, the two phases should occur with close to equal probabilities, while transitions between the phases will be infrequent (as is observed in Figure S1, Supporting Information). For the other replicas, at lower or higher temperatures, there is always one clearly dominating phase because the minimum corresponding to the solid-like or liquid-like phase, respectively, is much lower in free energy. In the bottom panel of Figure 2, we show the microcanonical caloric curve ($T(E)$), which is obtained by combining the estimates from the individual replicas (we note that all the individual estimates agree very well with the combined curve). As expected, the microcanonical caloric curve exhibits a S-bend in the phase coexistence region, from which the freezing (T_f) and melting temperatures (T_m) can be obtained. By averaging over last part of the simulation, we estimate the freezing and melting temperatures for the LJ147 cluster to be $T_f = 0.345(1)\ T^*$ and $T_m = 0.376(1)\ T^*$, respectively (see Figure S7, Supporting Information).

In Figure 3, we present the canonical caloric curve ($\langle E\rangle(T)$) (i.e., the average total energy in the canonical ensemble), standard deviation of the total energy in the canonical ensemble ($\sigma_E(T)$), and canonical specific heat ($C_v(T)$) obtained from the **LJ147-1** simulation. For comparison, we also show the microcanonical caloric curve in orange. We can note that for the curves presented in Figure 3, the error bars are negligible as

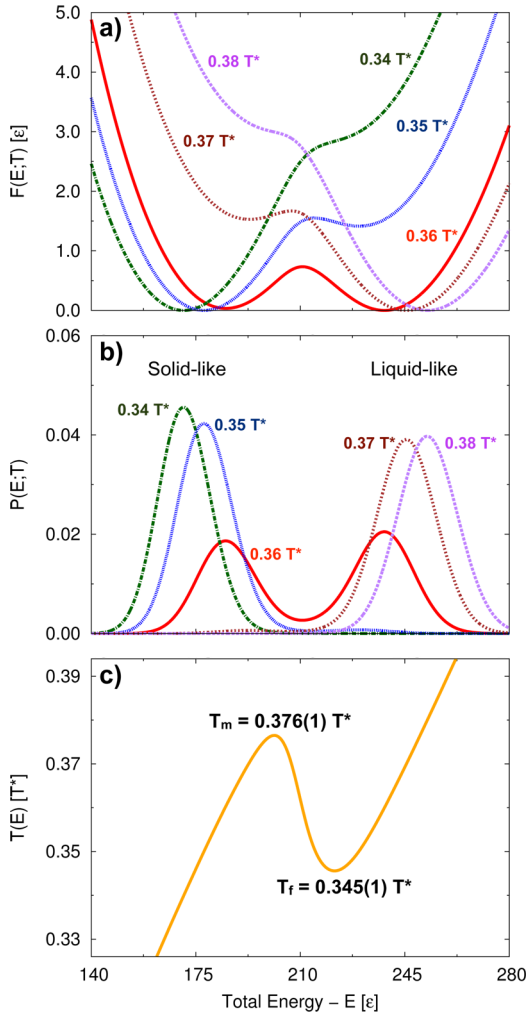

Figure 2. Phase coexistence region (**LJ147-1** results): (a) Total free energies $F(E;T)$. (b) Total energy probability distributions $P(E;T)$. (c) Microcanonical caloric curve $T(E)$, which is obtained by combining estimates from different replicas. The corresponding configurational quantities are shown in Figure S2 of the Supporting Information.

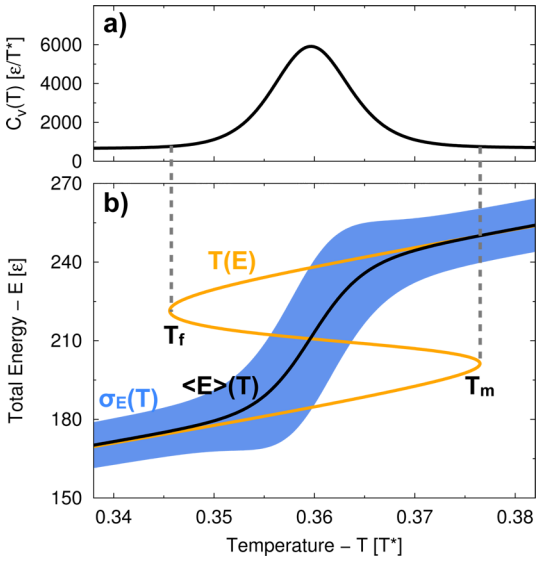

Figure 3. Phase coexistence region (**LJ147-1** results): (a) Canonical specific heat $C_v(T)$. (b) Canonical caloric curve $\langle E\rangle(T)$ (black line), standard deviation of the total energy in the canonical ensemble $\sigma_E(T)$ (blue shaded area), and microcanonical caloric curve $(T(E)$ (orange line, note that for this curve the independent variable, i.e., the total energy E, is on the vertical axis). The error bars for the curves are negligible (see Figure S4, Supporting Information).

curves obtained at different times over the last part of the simulation are indistinguishable from each other (see Figure S4, Supporting Information). We observe that, as expected, the average total energy rapidly increases as the cluster melts (i.e., the liquid-like phase becomes more dominating), while due to the enhanced fluctuations, the specific heat curve is characterized by a broad peak. We estimate the peak of the specific heat curve to be at a temperature of 0.360(1) T^* (see Figure S7, Supporting Information), which we know from above is the temperature where the two phases are almost equally probable. It is clearly observed that inside the phase coexistence region, the canonical and microcanonical caloric curves are very different from each other, which is one of the characteristics of the quasi-first-order phase transitions (see below for further discussion on this point).

5.2. Complete Thermodynamical Behavior. In our second PT-WTE simulation, we investigate the complete thermodynamical behavior of the LJ147 cluster and consider the results from the **LJ147-2** simulation. In this simulation, we employ 11 replicas with geometrically distributed temperatures in the range from 0.20 T^* to 0.45 T^* and a biasing factor of γ = 5. We note that a geometrical distribution of temperatures is, in general, not optimal for phase transitions as it assumes a constant specific heat.[19] Despite this, we obtain a satisfactory potential energy overlap between all replicas.

In Figure 4, we present the total free energies, total energy probability distributions, and microcanonical caloric curve obtained from the **LJ147-2** simulation (the corresponding configurational quantities are shown in Figure S3, Supporting Information). We notice that all replicas have one dominating phase, i.e., none of the replicas is close to the middle of the phase coexistence region, where the probability distribution would be bimodal. Furthermore, there are only two replicas close to the phase coexistence region, with temperatures 0.353 T^* and 0.383 T^*, and their probability distributions are effectively disjointed. Therefore, it would seem that the temperature distribution of the replicas is not favorable to describe the phase coexistence region. Nevertheless, the enhanced sampling provided by the PT-WTE approach results in a very good description of the phase coexistence region. As observed in Figure S6 of the Supporting Information, the **LJ147-2** simulation yields caloric and specific heat curves that are in good agreement with the results from **LJ147-1** simulation, although with slightly higher error bars. Furthermore, by averaging over the last part of the **LJ147-2** simulation (see Figure S7, Supporting Information), we estimate the freezing and melting temperatures to be T_f = 0.346(2) T^* and T_m = 0.376(3) T^*, respectively, and the peak of the specific heat curve to be at 0.360(3) T^*. These estimates are in good agreement with the results from the **LJ147-1** simulation. Therefore, although the **LJ147-2** simulation explores a much larger temperature range and employes more sparsely placed replicas, it still provides as good description of the phase coexistence region as the **LJ147-1** simulation that focused only on this critical region.

In Figure 5, we present the canonical caloric curve, standard deviation of the total energy in the canonical ensemble, canonical specific heat, and microcanonical caloric curve

dx.doi.org/10.1021/ct400859f | J. Chem. Theory Comput. 2013, 9, 5267−5276

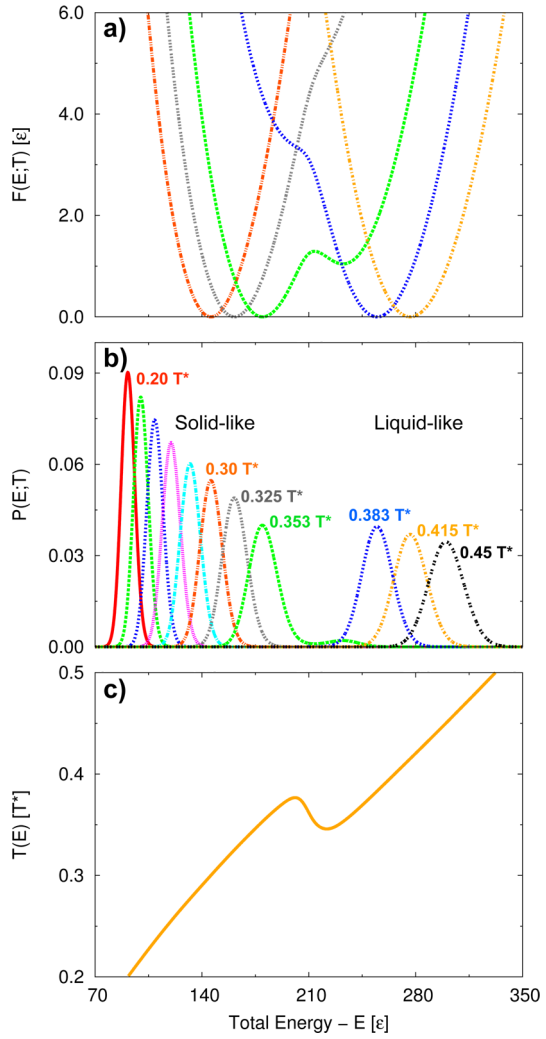

Figure 4. Complete thermodynamical behavior (**LJ147-2** results): (a) Total free energies $F(E;T)$ (for clarity, we do not show all replicas). (b) Total energy probability distributions $P(E;T)$. (c) Microcanonical caloric curve $T(E)$, which is obtained by combining estimates from the different replicas. The corresponding configurational quantities are shown in Figure S3 of the Supporting Information.

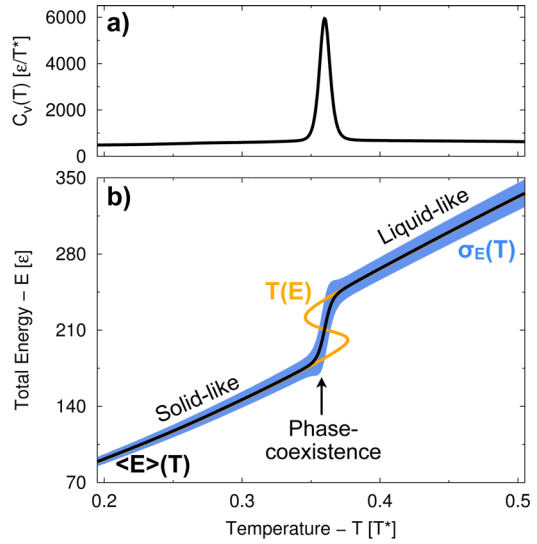

Figure 5. Complete thermodynamical behavior (**LJ147-2** results): (a) Canonical specific heat $C_v(T)$. (b) Canonical caloric curve $\langle E\rangle(T)$ (black line), standard deviation of the total energy in the canonical ensemble $\sigma_E(T)$ (blue shaded area), and microcanonical caloric curve $T(E)$ (orange line, note that for this curve the independent variable, i.e., the total energy E, is on the vertical axis). Note that the error bars of the curves are negligible on the scale employed in this figure (see Supporting Information).

obtained from the **LJ147-2** simulation (we note that on the scale employed in Figure 5, the error bars of the curves are negligible; see the Supporting Information). The results in Figure 5 show very clearly the thermodynamical behavior of the LJ147 cluster. Outside the phase coexistence region, the canonical caloric curve is almost linear for the two separate solid-like and liquid-like sections of the curve, while inside the phase coexistence region there is much more rapid increase in the average total energy as the cluster melts, and we go from the solid-like section to the liquid-like section of the curve. The phase coexistence region is identified by a clear peak in the specific heat curve, which is otherwise almost completely constant. Outside the phase coexistence region, the canonical and microcanonical caloric curves are exactly the same so the two different ensembles are equivalent. However, inside the phase coexistence region, the microcanonical canonical curve has the characteristic S-bend and thus differs from the canonical curve. Therefore, inside the phase coexistence region, the two different ensembles will not be equivalent, which is one of the peculiarities of quasi-first-order phase transitions. In the thermodynamic limit, the microcanonical and canonical ensemble must be equivalent, so the S-bend in the microcanonical caloric curve will even out as the size of the cluster is increased and eventually disappears in the thermodynamic limit.[12,31]

5.3. Obtaining the Free Energy Surface for Other Order Parameters. One interesting feature of the WTE is the possibility during post-processing to perform reweighting[32] of the free energies from the WTE and obtain the unbiased free energy surfaces for some other order parameters. In this section, we consider the **LJ147-1** simulation and show how this feature can be employed to obtain a further structural picture of the phase transition. We employ a global order parameter denoted as D_6 that is based on the extension of the Steinhardt order parameters[33] by Frenkel and co-workers[34,35] as explained in the Supporting Information. As shown below, the D_6 parameter is able to clearly distinguish between the two phases, with values larger and smaller than 0.5 characterizing the solid-like and liquid-like phases, respectively (see also Figures S8 and S9, Supporting Information).

In Figure 6, we present the free energy surfaces $F(U,D_6;T)$ as a function of the potential energy U and the D_6 parameter for the replicas from the **LJ147-1** simulation. For the replica at the lowest temperature of 0.34 T^*, only the free energy basin corresponding to the solid-like phase is visible (there is a small feature corresponding to the liquid-like phase that is more than 3 ε higher in free energy and therefore negligible). Then, as the temperature is increased, the free energy basin corresponding to the liquid-like phase starts to appear. For the replica at a temperature of 0.36 T^*, where the two phases are almost equally probable, we can clearly observe two different free energy basins. The basin corresponding to the liquid-like phase is shallower and much broader along the D_6 axis than the basin corresponding to the solid-like phase, so the liquid-like phase is characterized by a larger spread in the value of the D_6

dx.doi.org/10.1021/ct400859f | J. Chem. Theory Comput. 2013, 9, 5267−5276

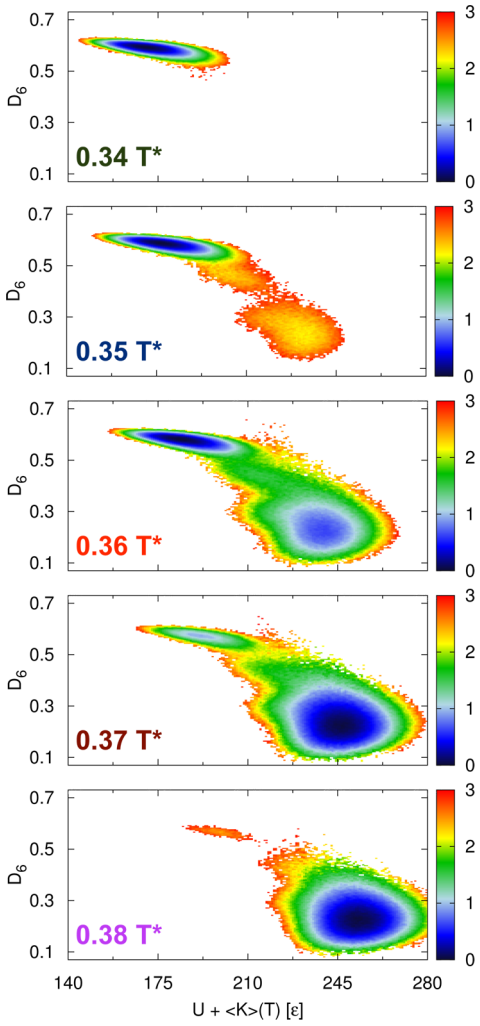

Figure 6. Free energy surfaces $F(U,D_6;T)$ as a function of the potential energy and the D_6 structural order parameter (see text and Supporting Information) for the replicas from the **LJ147-1** simulation. The surfaces are obtained by reweighting the free energies from the PT-WTE simulation. For each temperature, the potential energy scale has been shifted by the average kinetic energy, and the basin lower in free energy is defined to have a free energy of zero.

parameter (see also Figure S9, Supporting Information for the free energy as a function of D_6 parameter only). As the temperature is increased from 0.36 T^*, the free energy basin corresponding to the solid-like phase starts to disappear and has vanished at a temperature of 0.38 T^* (the feature corresponding to the solid-like phase is 2.5 ε higher in free energy and thus can be ignored). The results in Figure 6 are in line with our estimate of the freezing and melting temperatures of 0.345(1) T^* and 0.376(1) T^*, respectively. Only at temperatures from 0.35 T^* to 0.37 T^*, which are inside the phase coexistence region, do we clearly observe two free energy basins that correspond to the two different phases. At temperatures outside the phase coexistence region, 0.34 T^* and 0.38 T^*, only one basin, corresponding to the solid-like and liquid-like phases, respectively, can be observed (for both temperatures, the feature corresponding to the other phase is much higher in free energy and can be neglected).

6. DISCUSSION AND CONCLUSIONS

In this paper, we have explored the performance of the PT-WTE approach in obtaining a thermodynamical description of a molecular system. In particular, we considered a Lennard–Jones cluster that is a prototypical example of a finite-size system exhibiting a a quasi-first-order phase transition. Differently from their bulk counterparts, such phase transitions are characterized by range of temperatures where two distint phases are thermodynamically stable and coexist. Here, we considered two separate PT-WTE simulations: one that focused only on the phase coexistence region and employed densely spaced replicas and another that considered the complete thermodynamical behavior and employed more sparsly spaced replicas. Despite the more sparsely placed replicas, the **LJ147-2** simulation provided comparably accurate description of the critical phase coexistence region as the more focused **LJ147-1** simulation. The good agreement between the two simulations clearly indicates the quality of the PT-WTE results presented here. On the basis of the positive performance observed, we can definitely state that the PT-WTE approach is an effective option for estimating the density of states (or equivalently, the entropy) and thereby obtaining the thermodynamical properties of a given molecular system.

One issue that we did not examine in the current work is the selection of the temperature distribution for the PT-WTE replicas, which often is a critical issue in PT simulation.[19,36] Instead, we either employed equispaced temperatures or a geometrical distribution of temperatures. The case of the geometrical distribution is more significant, as this distribution assumes a constant specific heat and, therefore, is clearly not optimal for phase transitions. Despite this unfavorable temperature distribution, we obtained a satisfactory potential energy overlap, and the PT-WTE simulation yielded accurate results. It should be possible to increase the efficiency of the PT-WTE approach for phase transitions and in general by choosing a more sensible temperature distribution for the problem at hand.

The procedure presented in the current work should be easily extended to cases where the potential energy alone is not sufficient for obtaining accurate free energies, possibly due to a hysteresis behavior caused by an orthogonal degree of freedom not properly accounted for. There, we would need to perform well-tempered metadynamics simulations where the WTE is combined with some appropriately chosen collective variable s. This would yield free energy surfaces $F(U,s;T)$ that are functions of U and s. By integrating over the collective variable s, we can obtain the free energies as a function of the potential energy alone as $F_c(U;T) = -\beta^{-1} \ln \int ds e^{-\beta F(U,s;T)}$ and then obtain the thermodynamical properties in the same manner as presented in the current work.

Finally, we want to mention that the procedure presented in the current work is extendable to phase transitions in periodic systems. We are actively pursuing this direction, and this will be the subject of future publications.

■ ASSOCIATED CONTENT

Supporting Information

Configurational thermodynamical quantities for the PT-WTE simulations. Discussion on the error bars for the PT-WTE simulations. Information on the D_6 order parameter employed in the reweighting of the free energies. This material is available free of charge via the Internet at http://pubs.acs.org.

AUTHOR INFORMATION

Corresponding Author

*E-mail: omar.valsson@phys.chem.ethz.ch.

Notes

The authors declare no competing financial interest.

ACKNOWLEDGMENTS

O.V. thanks Ali Hassanali and Gareth Tribello for useful discussion. Furthermore, Gareth Tribello is thanked for help with the PLUMED 2.0 code. The authors thank Pratyush Tiwary for reading over the manuscript. All calculations were performed on the Brutus HPC cluster at ETH Zurich. We acknowledge the European Union Grant ERC-2009-AdG-247075 for funding.

REFERENCES

(1) Wang, F.; Landau, D. *Phys. Rev. Lett.* **2001**, *86*, 2050−2053.
(2) Berg, B.; Neuhaus, T. *Phys. Rev. Lett.* **1992**, *68*, 9−12.
(3) Kim, J.; Straub, J.; Keyes, T. *Phys. Rev. Lett.* **2006**, *97*, 050601.
(4) Bonomi, M.; Parrinello, M. *Phys. Rev. Lett.* **2010**, *104*, 190601.
(5) Barducci, A.; Bussi, G.; Parrinello, M. *Phys. Rev. Lett.* **2008**, *100*, 020603.
(6) Laio, A.; Parrinello, M. *Proc. Natl. Acad. Sci. U.S.A.* **2002**, *99*, 12562−12566.
(7) Micheletti, C.; Laio, A.; Parrinello, M. *Phys. Rev. Lett.* **2004**, *92*, 170601.
(8) Michel, C.; Laio, A.; Milet, A. *J. Chem. Theory Comput.* **2009**, *5*, 2193−2196.
(9) Hansmann, U. H. *Chem. Phys. Lett.* **1997**, *281*, 140−150.
(10) Sugita, Y.; Okamoto, Y. *Chem. Phys. Lett.* **1999**, *314*, 141−151.
(11) Deighan, M.; Bonomi, M.; Pfaendtner, J. *J. Chem. Theory Comput.* **2012**, *8*, 2189−2192.
(12) Wales, D. J. *Energy Landscapes: Applications to Clusters, Biomolecules and Glasses*; Cambridge University Press: Cambridge, 2003.
(13) Berry, R.; Jellinek, J.; Natanson, G. *Phys. Rev. A* **1984**, *30*, 919−931.
(14) Schmidt, M.; Kusche, R.; Hippler, T.; Donges, J.; Kronmüller, W.; von Issendorff, B.; Haberland, H. *Phys. Rev. Lett.* **2001**, *86*, 1191−1194.
(15) Buch, V.; Martonak, R.; Parrinello, M. *J. Chem. Phys.* **2005**, *123*, 051108.
(16) Buch, V.; Martonak, R.; Parrinello, M. *J. Chem. Phys.* **2006**, *124*, 204705.
(17) Amadei, A.; Apol, M. E. F.; Di Nola, A.; Berendsen, H. J. C. *J. Chem. Phys.* **1996**, *104*, 1560−1574.
(18) Sugita, Y.; Okamoto, Y. *Chem. Phys. Lett.* **2000**, *329*, 261−270.
(19) Earl, D. J.; Deem, M. W. *Phys. Chem. Chem. Phys.* **2005**, *7*, 3910−3916.
(20) Bussi, G.; Gervasio, F. L.; Laio, A.; Parrinello, M. *J. Am. Chem. Soc.* **2006**, *128*, 13435−13441.
(21) Kumar, S.; Rosenberg, J. M.; Bouzida, D.; Swendsen, R. H.; Kollman, P. A. *J. Comput. Chem.* **1992**, *13*, 1011−1021.
(22) Kim, J.; Keyes, T.; Straub, J. E. *J. Chem. Phys.* **2011**, *135*, 061103.
(23) Rizzi, L. G.; Alves, N. A. *J. Chem. Phys.* **2011**, *135*, 141101.
(24) Lynden-Bell, R. M.; Wales, D. J. *J. Chem. Phys.* **1994**, *101*, 1460−1476.
(25) Jones, J. E. *Proc. R. Soc. London, Ser. A* **1924**, *106*, 463−477.
(26) Northby, J. A. *J. Chem. Phys.* **1987**, *87*, 6166−6177.
(27) Pronk, S.; Pall, S.; Schulz, R.; Larsson, P.; Bjelkmar, P.; Apostolov, R.; Shirts, M. R.; Smith, J. C.; Kasson, P. M.; van der Spoel, D.; et al. *Bioinformatics* **2013**, *29*, 845−854.
(28) Tribello, G. A.; Bonomi, M.; Branduardi, D.; Camilloni, C.; Bussi, G. *Comput. Phys. Commun.* **2013**, DOI: 10.1016/j.cpc.2013.09.018.
(29) Bussi, G.; Donadio, D.; Parrinello, M. 2007, *126*, 014101.
(30) Kim, J.; Straub, J. E. *J. Chem. Phys.* **2010**, *133*, 154101.
(31) Wales, D. J.; Doye, J. P. K. *J. Chem. Phys.* **1995**, *103*, 3061−3070.
(32) Bonomi, M.; Barducci, A.; Parrinello, M. *J. Comput. Chem.* **2009**, *30*, 1615−1621.
(33) Steinhardt, P.; Nelson, D.; Ronchetti, M. *Phys. Rev. B* **1983**, *28*, 784−805.
(34) ten Wolde, P.-R.; Ruiz-Montero, M. J.; Frenkel, D. *Faraday Discuss.* **1996**, *104*, 93−110.
(35) Auer, S.; Frenkel, D. *J. Chem. Phys.* **2004**, *120*, 3015−3029.
(36) Katzgraber, H. G.; Trebst, S.; Huse, D. A.; Troyer, M. *J. Stat. Mech.* **2006**, P03018−P03018.